

# An X-ray view of the INTEGRAL/IBIS blazars

S. Gianni<sup>1,2\*</sup>, A. De Rosa<sup>2</sup>, L. Bassani<sup>3</sup>, A. Bazzano<sup>2</sup>, T. Dean<sup>4</sup> and P. Ubertini<sup>2</sup>

<sup>1</sup> *Università di Roma Tor Vergata*

<sup>2</sup> *INAF-IASF Roma*

<sup>3</sup> *INAF-IASF Bologna*

<sup>4</sup> *School of Physics and Astronomy, University of Southampton, SO17 1BJ, UK*

Accepted 2009 ... . Received 2009 ... ; in original form ...

## ABSTRACT

Aim of this work is a broad-band study with INTEGRAL, Swift and XMM-Newton satellites of a sample of 9 blazars (7 FSRQ and 2 BL Lac) with redshift up to about 4.

The spectral analysis has shown clear evidence of a flattening of the continuum towards the low energies ( $E < 3$  keV observer frame). This behaviour is well reproduced both with an absorbed power-law model ( $N_H \sim 10^{20}$ - $10^{23}$  cm<sup>-2</sup> in the rest-frame of the sources) or a broken power-law continuum model (with an energy break below 3 keV in the observer-frame). No Compton reflection features, Fe  $K\alpha$  line and hump at high energies, have been detected, with the exception of the source IGR J22517+2218 that shows the presence of a weak iron line.

In this work we also investigate a possible correlation between the absorption column density  $N_H$  and the red-shift.

We confirm the existence of a  $N_H$ - $z$  trend, with the higher absorption at  $z > 2$  for a larger sample compared to previous results. The distribution of the  $N_H$  and the photon index  $\Gamma$  is also presented. The hard X-ray data allow us to detect highly absorbed sources (with  $N_H \geq 10^{23}$  cm<sup>-2</sup> in rest-frame of the source) characterized by photon index distribution peaked at harder values ( $\Gamma \sim 1.4$ ) with respect to that obtained with XMM data only ( $\Gamma \sim 2$ ).

**Key words:** galaxies: active – X-rays: galaxies – quasars: general.

## 1 INTRODUCTION

Blazars are one of the most intriguing class of objects among the Active Galactic Nuclei (AGN) and include BL Lacertae objects (BL Lac) and Flat-Spectrum Radio Quasars (FSRQ). The intrinsic differences between these two types of sources are in their optical spectra and in the intensity of their emission: a BL Lac source does not show any optical emission lines ( $EW < 5\text{\AA}$ ) and it is basically a low-power blazar ( $L_{Bol} \sim 10^{46} - 10^{47}$  erg s<sup>-1</sup>), whereas a FSRQ source shows significant emission line equivalent widths and corresponds to a high-power blazar ( $L_{Bol} \sim 10^{48}$  erg s<sup>-1</sup>) (Stickel et al. 1991; Padovani 1997). In the AGN unified scheme (Antonucci 1993), blazars are interpreted as radio-sources with a relativistic jet aligned along the line of sight (Urry & Padovani 1995); in other words, the class of blazars is represented by Radio Loud (RL) AGN observed very close to the direction of the relativistic jets ( $< 10^\circ$ ).

The Spectral Energy Distribution (SED) of blazars

is usually modelled with two large humps produced via Synchrotron (peaking in the infra-red to soft X-ray energy band) and Inverse Compton (IC) emission, dominating the hard X-ray to gamma-ray regimes, respectively. The lower energy emission component is Synchrotron radiation from the jet whereas the high-energy component arises through the inverse Compton of soft photons by highly relativistic electrons in the jet plasma. These soft photons originate from the local Synchrotron radiation within the jet or the nuclear optical/UV emission, namely Synchrotron Self-Compton (SSC) and External Compton (EC) components, respectively (see Maraschi, Ghisellini & Celotti 1992; Dermer & Schlickeiser 1993; Sikora, Begelman & Rees 1994).

The X-ray spectrum of an AGN is usually well described by a power-law with a specific flux (i.e. per unit energy interval) of the form  $N(E) \propto E^{-\Gamma}$ , where  $E$  is the energy,  $N(E)$  is the number of photons in units of s<sup>-1</sup> cm<sup>-2</sup> keV<sup>-1</sup> and  $\Gamma$  is the *photon index*. However, X-ray spectra of blazars show some deviations from the simple power-law. These spectral signatures appear in the soft X-ray band with a curvature (a

\* E-mail:...

flattening or a steepening of the spectrum); in addition, the presence of Compton reflection components in RL objects is still debated.

A clear physical interpretation of these features has not yet been found. In the present work, we investigate these still open questions in order to achieve a better understanding of the general properties of the blazars spectra. The state-of-art of the study of these important issues can be summarize as follows:

(i) Two physical interpretations to the flattening of the primary intrinsic continuum with respect to a simple power-law exist so far (Page et al. 2005; Galbiati et al. 2005; Yuan et al. 2006): absorption in excess of the Galactic component (e.g. Cappi et al. 1997; Yuan et al. 2006) and a break in the intrinsic continuum (Sikora, Begelman & Rees 1994; Tavecchio et al. 2007). For the absorption excess, a dependence between the hydrogen column density of the absorber ( $N_H$ ) and the redshift  $z$  has been proposed. In fact in a former work by Yuan et al. (2006) based on XMM observations of a sample of 32 RL sources, a  $N_H$ - $z$  correlation has been found.

(ii) Contrary to Radio Quiet (RQ) sources the presence of reflection features - most notably the Fe  $K\alpha$  line and the associated Compton reflection "hump" at about 20 – 30 keV - from the cores of the RL AGN is not well established. In particular, the reprocessed features are generally intense and always detected in RQ AGN (Matt 2001), whereas in RL AGN the iron line and the reflection component can be absent or weak. X-ray observations of RL AGN with ASCA, RXTE and Beppo SAX (e.g. Sambruna, Eracleous & Mushotzky 1999; Eracleous, Sambruna & Mushotzky 2000; Grandi et al. 2001; Ballantyne, Ross & Fabian 2002; Grandi & Palumbo 2004; Grandi, Malaguti & Fionchi 2006) have shown that some of these objects (defined as Broad Line Radio Galaxies) seem to have weak hard X-ray reflection features.

In this paper we present a broad-band (0.2 – 100 keV) study of a sample of 9 blazars up to redshift  $\sim 4$  observed with INTEGRAL, Swift and XMM-Newton satellites. The wide energy range covered by the instruments is well suited to better address their spectral behaviour.

In Sections 2.1-2.4 we present the data set and analysis, while in Section 3.1 we show the details of the spectral analysis. The results are discussed in Section 3.2 and in Section 3.3 a study of the distribution of different spectral parameters and possible correlation is discussed and finally, we summarize the results in Section 4.

## 2 OBSERVATIONS AND DATA REDUCTION

### 2.1 THE HARD-X RAYS SELECTED SAMPLE

The INTEGRAL/IBIS total sample is derived from the third IBIS/ISGRI survey catalog that included 421 sources for a total exposure time of 40Ms; 131 sources out of 421 have been identified as AGN. The survey input data set consists of all pointing data available at the end of 2006 May, from revolutions 12-429 inclusive, covering the time period from launch (17 October 2002) to the end of 2006 April. Details about this survey are presented by Bird et al. (2007). A sub-

set of sources has been selected according with the following selection criteria:

- sources classified as blazars, optically identified (e.g. Masetti et al. 2004, 2008)
- sources also observed in the soft X-ray energy domain (0.2 – 10 keV);

Two further sources 3C 273 and 4C 04.42 have been excluded since widely discussed elsewhere (Chernyakova et al. 2007; De Rosa et al. 2008).

Our sample of INTEGRAL selected blazars, is composed of 9 sources: 7 FSRQ objects with  $0.53 < z < 3.67$  and 2 BL Lac objects with  $z \sim 0.07$  and 0.09, but only five out of seven FSRQ were available at the time of our analysis. For the 2 other objects we adopted the hard X-rays BAT data.

Relevant information on the sample are reported in Table 1 where we list the source name, type, optical coordinates, redshift, Galactic absorption along the line of sight according to Dickey & Lockman (1990). In the last column of Table 1 we also list the IBIS 20 – 100 keV flux as reported by Bird et al. (2007) and the BAT 14 – 195 keV flux as reported by AGN Catalog of the first 9 months available at the time we started this project <sup>1</sup>.

We remark that source with IGR name (IGR J22517+2218) is discovered in hard X-ray with INTEGRAL. It is the farthest object so far detected by INTEGRAL whose nature was determined *a posteriori* through optical spectroscopy (Bassani et al. 2007). It is worth to note that two sources (FSRQs 3C 279 and PKS 1830-211) have been detected in the Gamma Ray band with the Astro-rivelatore Gamma a Immagini Leggero (AGILE) <sup>2</sup> (Giuliani et al. 2009; Tavani et al. 2008; Pittori et al. 2009) and the Large Area Telescope on board the Fermi Gamma-ray Large Area Space Telescope (GLAST) <sup>3</sup>. The latter satellite also revealed a third source belonging to our sample, the object BL Lac (Abdo et. al 2009).

### 2.2 INTEGRAL DATA

The INTEGRAL data presented here are based on pointings with the IBIS instrument (Ubertini et al. 2003), collected over the period from end of 2002 up to April 2006 (revolution 12 up to 429). Images from the ISGRI detector (Lebrun et al. 2003) for each pointing have been generated in different energy bands using off-line scientific Analysis Software (Goldwurm et al. 2003) OSA version 5.1. Count

<sup>1</sup> The BAT data have been taken from the on-line archive at: <http://swift.gsfc.nasa.gov/docs/swift/results/bs9mon>. For the BAT spectra (related to PKS 2149-306 and 0537) we stress that in the 22-months survey now available, the 15-45 keV fluxes are doubled with respect to the 9-months survey. This effect is taken into account with the cross calibration constant that has been added when dealing with the fit between soft-X and hard-X rays spectra.

<sup>2</sup> An Italian Space Agency (ASI) mission launched on 23 April 2007 with a key scientific project: the Gamma-Ray observations of blazars.

<sup>3</sup> An international and multi-agency mission launched on 11 June 2008; one of its major scientific goals is to provide new data on the Gamma-ray activity of AGN.

**Table 1.** Data for our sample of blazars observed with INTEGRAL, Swift and XMM-Newton.

| <i>Source</i>      | <i>Type</i> | <i>Broad – Band</i> | R.A.        | Dec         | <i>redshift</i> | $N_H^{Gal}$<br>[ $10^{22} \text{ cm}^{-2}$ ] | $F_{20-100 \text{ keV}}^{IBIS}$<br>( $F_{14-195 \text{ keV}}^{BAT}$ )<br>[ $10^{-11} \text{ erg} \cdot \text{cm}^{-2} \cdot \text{s}^{-1}$ ] | $L_{20-100 \text{ keV}}^{rest-frame}$<br>( $L_{14-195 \text{ keV}}^{rest-frame}$ )<br>[ $10^{46} \text{ erg} \cdot \text{s}^{-1}$ ] |
|--------------------|-------------|---------------------|-------------|-------------|-----------------|--|--|---|
| QSO B0836+710      | FSRQ        | XMM+INTEGRAL        | 08 41 24.37 | +70 53 42.2 | 2.172           | 0.030  | 6  | 63.1  |
| 1ES 0033+595       | BL Lac      | XMM+INTEGRAL        | 00 35 52.63 | +59 50 04.6 | 0.086           | 0.427  | 2  | 0.1   |
| PKS 0537-286       | FSRQ        | XMM+BAT             | 05 39 54.28 | -28 39 55.9 | 3.104           | 0.020  | (3)  | (31.6)  |
| PKS 2149-307       | FSRQ        | XMM+BAT             | 21 51 55.52 | -30 27 53.7 | 2.345           | 0.020  | (5)  | (39.8)  |
| Swift J1656.3-3302 | FSRQ        | XRT+INTEGRAL        | 16 56 16.56 | -33 02 09.3 | 2.4             | 0.220  | 2  | 50.1  |
| IGR J22517+2218    | FSRQ        | XRT+INTEGRAL        | 22 51 53.50 | +22 17 37.3 | 3.668           | 0.050  | 4  | 100.0   |
| BL Lac             | BL Lac      | XRT+INTEGRAL        | 22 02 42.72 | +42 17 16.8 | 0.069           | 0.022  | 3  | 0.1   |
| PKS 1830-211       | FSRQ        | XMM+INTEGRAL        | 18 33 39.89 | -21 03 39.8 | 2.507           | 0.260  | 5  | 100.0   |
| 3C 279             | FSRQ        | XRT+INTEGRAL        | 12 56 11.17 | +05 47 21.5 | 0.536           | 0.020  | 2  | 2.5   |

rates at the source position have been extracted from individual images to provide light curves in different energy bands. From light curves the average fluxes have been derived and combined to produce an average source spectrum (for details see Bird et al. 2007) in the 20 – 100 keV band.

### 2.3 XMM-NEWTON DATA

XMM data of the six blazars (1ES 0033+595, 4C 04.42, PKS 1830-211, QSO B0836-710, PKS 0537-286 and PKS 2149-307) are a combination of proprietary data and public observations obtained from the XMM-Newton Science Archive<sup>4</sup>. The raw EPIC Observation Data Files (ODFs) were obtained from the XMM Science Archive and reduced using the standard Science Analysis System (SAS) software package (v.7.1.0) and the most recent calibration files available at the time of the data reduction. We used the EMCHAIN and EPCHAIN task for the pipeline processing of the ODFs to generate the corresponding event files. The spectra were created using X-ray events of pattern 0-12 for MOS and 0-4 for PN. The source counts were extracted from a circular region centred on the source with a radius of 20-40 arcsec and the background was derived from two nearby source-free circular regions of the same size. Spectra were re-binned using GRPPHA to have a minimum of 20 counts in each bin<sup>5</sup>, so that the  $\chi^2$  statistic could reliably be used. Details of the XMM-Newton observations and the source observed count rates are summarized in Table 2.

### 2.4 SWIFT/XRT DATA

Swift/XRT data reduction of four blazars (3C 279, BL Lac, IGR J22517+2218, Swift J1656.3-3302) was performed using the tool XSELECT v. 2.4. Events for spectral analysis were extracted within a circular region of radius 20 arcsec centred on the source position. The background was extracted from

a circular region with the same radius and located far off the source. In all cases, the spectra were binned using GRPPHA. We used Ancillary Response Files (ARFs) and Response Matrix Files (RMFs) available for download from the HEASARC Calibration Database (caldb) calibration files at: [http://heasarc.gsfc.nasa.gov/docs/heasarc/caldb/caldb\\_intro.html](http://heasarc.gsfc.nasa.gov/docs/heasarc/caldb/caldb_intro.html). Table 3 lists the observation ID, the observation start time, the integration time and the observed count rate.

### 3 BROAD-BAND SPECTRAL ANALYSIS

The spectral analysis was performed by combining the different data from each instrument using the X-ray SPECTral fitting software XSPEC v. 11.3.2 (Arnaud 1996). The errors are quoted at 90% confidence level for one interesting parameter. The energy values are always given in the observer frame, if not otherwise specified. Throughout this paper, a WMAP (Wilkinson Microwave Anisotropy Probe) Cosmology of  $H_0 = 70 \text{ km s}^{-1} \text{ Mpc}^{-1}$ ,  $\Omega_\lambda = 0.73$  and  $\Omega_m = 1 - \Omega_\lambda$  is assumed.

We have combined XMM spectrum with the IBIS one for the blazars 1ES 0033+595, 4C 04.42, PKS 1830-211, QSO B0836-710; XRT spectrum with the IBIS one for 3C 279, BL Lac, IGR J22517+2218, Swift J1656.3-3302 and XMM spectrum with the BAT one for PKS 0537-286, PKS 2149-307 (see Table 1).

To account for possible cross-calibration mismatches between different instruments as well as to take into account flux variations between the observing periods, a multiplicative constant factor (C) has always been added to the fit. In general, the calibration between the various satellites is performed analyzing the Crab spectrum. In particular, various studies of the Crab spectrum (e.g. Kirsch et al. 2004, 2005) have shown that the inter-calibration XMM/INTEGRAL and Swift/INTEGRAL is close to 1 (within a few percent). We remark that, since XMM, Swift and INTEGRAL observations were not simultaneous, flux variations are also possible according to the blazar-nature of objects. Being the inter-calibration constant  $C \sim 1$ , we suggest that, a different value for this constant is likely due to flux variability. In

<sup>4</sup> <http://xmm.esac.esa.int/xsa/index.shtml>.

<sup>5</sup> 10 counts are the minimum number of counts required to use the  $\chi^2$  minimization technique.

**Table 2.** XMM-Newton observations log and source observed count rates.

| <i>Source</i> | Obs.ID     | Date of obs. | Exp. time<br>MOS1<br>(s) | Exp. time<br>MOS2<br>(s) | Exp. time<br>PN<br>(s) | Counts/s<br>MOS1<br>(0.2 – 10keV)<br>(s <sup>-1</sup> ) | Counts/s<br>MOS2<br>(0.2 – 10keV)<br>(s <sup>-1</sup> ) | Counts/s<br>PN<br>(0.2 – 10keV)<br>(s <sup>-1</sup> ) |
|---------------|------------|--------------|--------------------------|--------------------------|------------------------|---|---|---|
| 1ES 0033+595  | 0094381301 | 2003-02-01   | 1204                     | 1535                     | 4209                   | 1.39 ± 0.04   | 1.39 ± 0.04   | 3.61 ± 0.03   |
| PKS 1830-211  | 0204580301 | 2004-03-24   | 30445                    | 30444                    | 20906                  | 0.58 ± 0.01   | 0.58 ± 0.01   | 1.65 ± 0.01   |
| QSO B0836-710 | 0112620101 | 2001-04-12   | 35614                    | 35620                    | 29035                  | 3.88 ± 0.01   | 3.85 ± 0.01   | 11.97 ± 0.02  |
| PKS 0537-286  | 0206350101 | 2005-03-20   | 80610                    | 80765                    | 64661                  | 0.205 ± 0.002   | 0.226 ± 0.002   | 0.746 ± 0.004   |
| PKS 2149-307  | 0103060401 | 2001-05-01   | 23959                    | 23960                    | 20287                  | 0.63 ± 0.01   | 0.62 ± 0.01   | 1.67 ± 0.01   |

**Table 3.** Swift/XRT observations log and source observed count rates.

| <i>Source</i>      | Obs.ID      | Date of obs. | Exp. time<br>XRT<br>(s) | Counts/s<br>XRT<br>(0.2 – 10keV)<br>(s <sup>-1</sup> ) |
|--------------------|-------------|--------------|-------------------------|--|
| BL Lac             | 00090042010 | 2008-08-29   | 5806                    | 0.20 ± 0.01  |
| IGR J22517+2218    | 00036660001 | 2007-05-26   | 8300                    | 0.054 ± 0.003  |
| Swift J1656.3-3302 | 00035272002 | 2006-06-13   | 4785                    | 0.075 ± 0.004  |
| 3C 279             | 00035019009 | 2008-11-26   | 22580                   | 0.198 ± 0.003  |

our analysis, this constant C between the two instruments at low and high energies has been allowed to vary freely in the fits. In particular, we have considered the MOS1 and XRT instruments as reference detectors in the case of XMM-INTTEGRAL or BAT data and XRT-INTTEGRAL data, respectively. Therefore, the inter-calibration constants in our fitting procedure are MOS2/MOS1, PN/MOS1, INTEGRAL/MOS1, BAT/MOS1 and INTEGRAL/XRT. However MOS2/MOS1 and PN/MOS1 are always  $\sim 1$  within few percent.

### 3.1 SPECTRAL FITTING RESULTS

To reproduce the shape of the intrinsic continuum of our sources we fitted the combined spectra (0.2 – 100 keV) of each source with several models.

Firstly, we fit the spectra of our sources in the 3 – 100 keV energy band with the model A, that corresponds to a simple power-law absorbed by gas of the Milky Way. The results of the fit are summarized in Table 4. The model A provides a good fit for all sources. When extrapolating this

model to the low energy range, a very poor fit in all cases but one (PKS 2149-307) was obtained; in fact the data to model ratio (see Figure 1) shows a clear systematic residuals below  $\sim 3$  keV in the observer frame. From the ratios shown in Figure 1, we can see that the spectra of the majority of the sources clearly show a deficit of soft X-ray counts with respect to the simple power-law model, indicating the possible presence of excess absorption and/or of an energy break in the intrinsic continuum.

In order to properly reproduce such a feature we tested the impact of different models.

In the model B we added an extra-absorption in the rest-frames of the sources (phabs\*zphabs\*zpo model in XSPEC) and results are presented in Table 5.

All sources of our sample, with the exception of PKS 2149-307 and PKS 1830-211, were well fitted with the model B, while for the source PKS 2149-307 we have obtained an upper limit value on the intrinsic absorbing column density and for PKS 1830-211 only a poor quality fit to the data has been derived. Details on this source will be discussed later in this section.

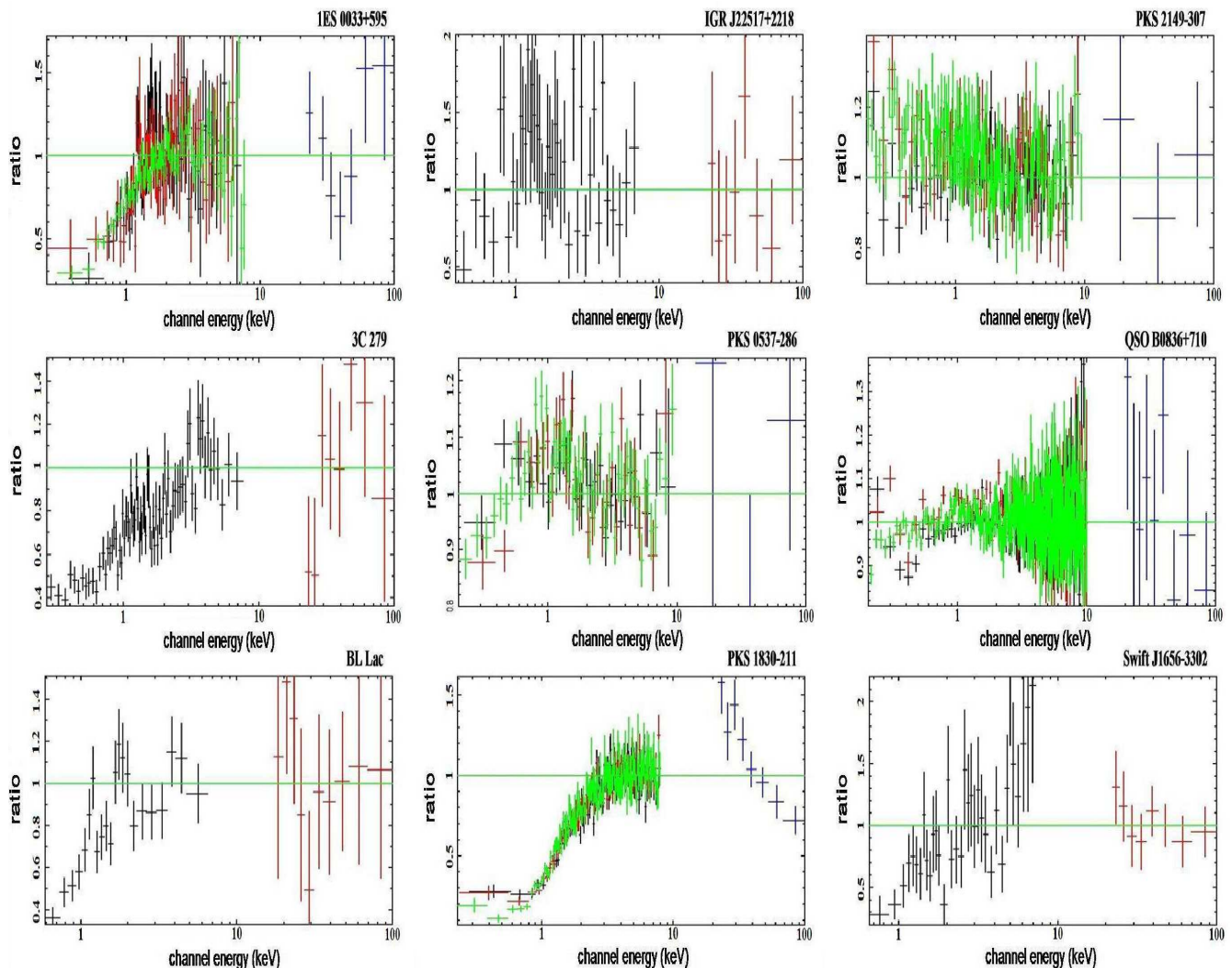


**Figure 1.** The data to model A ratio as obtained by fitting a simple power-law over the observed frame 3 – 100 keV energy range, and extrapolating over the 0.2 – 100 keV range. The black, red and green bins up to 10 keV are the data of MOS1, MOS2 and PN instruments, respectively.

Then, we tested a broken power-law continuum model C (phabs\*bknpo model in XSPEC) for the whole sample. Results are shown in the Table 6. This model did not improve the fit further in most of the cases and, also in those cases for which a slightly better  $\chi^2$  is obtained, the null hypothesis probability increases only a few per cent with respect to model B. Although strong statistical evidence does not exist for a broken power-law respect to the absorbed one, however the presence of an intrinsic spectral break cannot be ruled out.

For PKS 1830-211, both models B and C fail to reproduce source data. PKS 1830-211 is a gravitationally lensed galaxy and the excess absorption can be attributed to the intervening galaxy at redshift  $z = 0.89$ . The best-fit of the observed spectrum requires both an absorber and a broken power-law (model D), confirming the results reported by Zhang et al. (2008) with three XMM-Newton observations

Obs.ID 0204580201, 0204580301 and 0204580401<sup>6</sup> and the INTEGRAL average data (up to April 29, 2006). In fact, in addition to the excess cold absorption, PKS 1830-211 also exhibits an energy break at about 4 keV in the observer frame. Moreover, our result for the absorption in excess to the Galactic one, is in agreement with that obtained previously by De Rosa et al. (2005) with Chandra observations and a subset of the actual IBIS data. Table 7 reports the results of our best-fit model.

Finally, we also checked a Compton reflection component with a power-law reflected from neutral matter (pexrav model in XSPEC, Magdziarz & Zdziarski (1995)); the reflection component is parameterized in terms of  $R = \Omega/2\pi$ , the solid angle in units of  $2\pi$  subtended by the reflecting matter, assumed to be observed face-on). This model resulted in a worst fit and upper limit values on  $R$  for all absorbed sources (see Table 8).

<sup>6</sup> In our analysis we have chosen the observation with longer exposure time.

In addition, we have searched for the presence of an iron emission in the spectra of our sources. To this aim, we adopted the following method: we exclude the Fe K band, fit a continuum, then freeze the continuum, after we include the Fe K band and perform the fit again. The comparison between the values of the  $\chi^2$  of the fits performed including and excluding the Fe K band provides us a clear indication for the real presence of this feature of the observed spectra.

For all sources, but one (IGR J22517+2218), the application of this method does not produce any clear evidence for the presence of this feature in the spectrum. The main results for the source IGR J22517+2218 can be summarized as follows: the first step described before resulted in a photon index  $\Gamma=1.5$  and an upper limit on  $N_H=5\times 10^{22}$  cm $^{-2}$  with  $\chi_r^2/\text{dof}=23/29$ ; in the second step we included the iron channels and then we added a narrow line ( $\sigma=0.01$  keV) and the fit has been repeated obtaining  $\chi_r^2/\text{dof}=37/44$  with a probability  $P_{Ftest} > 99.7\%$  implying that this feature is real with an Equivalent Width  $EW=80 \pm 50$  eV; repeating the fit with a free photon index a value of  $\Gamma = 1.6 \pm 0.2$  is obtained with an iron line that is significant at the 99%. In summary, for this source there is the evidence for the presence of a weak line significant at the 99% level.

As a conclusion, we firmly asses that the an iron emission line is not request by our data, with the exception of the source IGR J22517+2218.

### 3.2 DISCUSSION

Our broad-band spectral analysis has shown that a deficit of photons in the soft X-ray energy domain is a common feature in our sample. This phenomenon has been previously observed in several samples of RL objects (e.g. Page et al. 2005; Galbiati et al. 2005; Yuan et al. 2006) and its origin is not yet well understood. It can be produced by either an intrinsically curved continuum or an extra absorption component.

The broken continuum hypothesis is linked to the blazar-type source. In fact, in the hypothesis of an intrinsically curved blazar continuum, one can assume that the relativistic electrons in the jet follow a broken power-law energy distribution with a low energy cut-off, producing a flattening in the observed spectrum. This is a purely phenomenological form assumed to reproduce the observed shape of the blazar SEDs, without any specific assumption on the acceleration/cooling mechanism acting on the particles (e.g. Tavecchio et al. 2007). Alternatively, it can be also assumed there is an inefficient radiative cooling of lower energy electrons of the jet producing a few Synchrotron photons to be scattered at higher energies (e.g. Sikora, Begelman & Rees 1994).

We emphasize that on basis of our spectral analysis an intrinsic spectral break cannot be ruled out (see the values of the reduced  $\chi^2$  and of the null hypothesis probability listed in the Tables 5 and 6). In this context, we just noted that the existence of a break in the intrinsic continuum is tightly related to the electron distribution, but important constraints on the curved electron distribution can be derived only analyzing both Synchrotron and EC components in the SED, that is out of the aim of present work. Therefore we will focus the following discussion on the absorption scenario.

The absorption explanation takes into account an absorbing gas in excess of the Galactic one; in some cases, the absorbing medium can be cold (not ionized) and located either between the observer and the source along the line of sight at a different redshift with respect to the blazar (e.g. Cappi et al. 1997; Fiore et al. 1998; Fabian et al. 2001; Masetti et al. 2004), or at the same redshift of the source (e.g. Page et al. 2005; Yuan et al. 2006) and it is namely an intrinsic cold absorber.

For an absorber located at several redshifts between the observer and the source, the damped Ly-alpha systems are the more plausible cause (e.g. Elvis et al. 1994) and the line of sight would have to pass through two or more very high column density damped Ly-alpha systems (e.g. Fall & Pei 1995). However, this is a rare occurrence (e.g. O’Flaherty & Jakobsen 1997; Zwaan, Verheijen & Briggs 1999) and favours the hypothesis of an intrinsic absorber with column densities of the order  $10^{22} - 10^{23}$  cm $^{-2}$ . An intrinsic origin is also confirmed by the soft X-ray spectral flattening detected so far only in radio loud objects (Bechtold et al. 1994; Reimers et al. 1995; Siebert et al. 1996).

The intrinsic hypothesis also suggests that the medium could be "warm" at the same stage. In this case, the absorbing medium, at the same redshift of the AGN (probably, the inner part of the dense interstellar medium of the young host galaxy), is ionized as due to the proximity from the jet (e.g. Fabian et al. 2001; Yuan et al. 2006).

For our sample, the fitting procedure supports the presence of an intrinsic (local to the AGN) cold absorber for all sources. Nevertheless a warm absorber model (absorbi in XSPEC) can be excluded since the model with an ionized-gas produces a worse fit and an inconsistent value for the ionization parameter ( $\xi \sim 0$  erg cm s $^{-1}$  and  $\xi > 500$  erg cm s $^{-1}$ , values indicating a neutral absorber and a completely ionized absorber, respectively).

The information on the absorption is of crucial importance to understand the blazar environment and its interaction with the jet.

Absorption originating from the material present in the AGN environment seems to be a more convincing explanation for many sources belonging to the class of RL AGN (Page et al. 2005; Yuan et al. 2006, and references therein). There is some evidence not only of absorption but also of a correlation between absorption and redshift, with the more distant sources being more absorbed and the increase in  $N_H$  with  $z$  occurring starting at  $z \sim 2$  (Yuan et al. 2006). We note that more than half of the sources in our sample appear in agreement with this scenario, since this fraction of objects has a redshift larger than 2.

As far it concerns the nature of this absorber, we suggest it could be associated to the presence of gas in the host galaxy illuminated by the blazar jet.

The excess of intrinsic absorption in the rest-frame of the RL objects compared with the lack of absorption above the Galactic value of their RQ counterparts (Canizares & White 1989; Lawson & Turner 1997; Yuan et al. 1998; Page et al. 2003, 2005; Vignali et al. 2003, 2005; Grupe et al. 2006), suggests that an intrinsic difference could exist in the local environments of the two classes of objects. Since the X-ray spectra of RL AGN appear to be dominated by the emission of the jet component, most

**Table 4.** Best fit parameters of a simple power-law model in 3-100 keV energy range.

| Model A            |                       |                         |                        |                      |                           |                |
|--------------------|-----------------------|-------------------------|------------------------|----------------------|---------------------------|----------------|
| Name               | ${}^1F_{ob(3-10keV)}$ | ${}^1F_{ob(20-100keV)}$ | ${}^3\Gamma$           | ${}^4C$              | ${}^5\chi_r^2/\text{dof}$ | ${}^6P_{null}$ |
| QSO B0836+710      | 4.1                   | 5.2                     | $1.34 \pm 0.02$        | $0.28 \pm 0.03$      | 0.91/1521                 | 0.996          |
| 1ES 0033+595       | 1.1                   | 1.5                     | $2.52^{+0.18}_{-0.17}$ | $4.2^{+2.5}_{-1.6}$  | 0.79/53                   | 0.865          |
| PKS 0537-286       | 0.5                   | 2.3                     | $1.19 \pm 0.06$        | $0.6 \pm 0.2$        | 1.05/329                  | 0.253          |
| PKS 2149-307       | 0.6                   | 4.9                     | $1.41 \pm 0.06$        | $1.9 \pm 0.5$        | 0.91/225                  | 0.835          |
| PKS 1830-211       | 1.4                   | 4.4                     | $1.22 \pm 0.04$        | $0.5 \pm 0.1$        | 1.03/442                  | 0.315          |
| Swift J1656.3-3302 | 0.5                   | 2.1                     | $1.60^{+0.33}_{-0.32}$ | $1.6^{+2.0}_{-0.9}$  | 1.02/18                   | 0.434          |
| IGR J22517+2218    | 0.3                   | 3.8                     | $1.43^{+0.59}_{-0.56}$ | $4.1^{+11.4}_{-3.1}$ | 0.66/14                   | 0.817          |
| Bl Lac             | 0.6                   | 2.3                     | $2.01^{+0.43}_{-0.41}$ | $4.3^{+6.5}_{-2.6}$  | 0.59/11                   | 0.840          |
| 3C 279             | 0.5                   | 2.1                     | $2.00^{+0.24}_{-0.23}$ | $4.3^{+3.1}_{-1.8}$  | 1.06/19                   | 0.382          |

<sup>1</sup> Observed flux in the 2 – 10 keV (or 20 – 100 keV) energy range in units of  $10^{-11}$  erg  $\text{cm}^{-2}$   $\text{s}^{-1}$ . <sup>3</sup> Photon index, related to the spectral index  $\alpha$  (where  $F_\nu \propto \nu^{-\alpha}$ ) by  $\alpha = \Gamma - 1$ . <sup>4</sup> IBIS/MOS, BAT/MOS or IBIS/XRT cross-calibration constant. <sup>5</sup> Reduced chi-squared to degrees of freedom. <sup>6</sup> Null hypothesis probability that is the probability of getting a value of  $\chi^2$  as large or larger than observed if the model is correct. If this probability is small then the model is not a good fit to the data.

**Table 5.** Best fit parameters of an absorbed power-law model in 0.2-100 keV energy range.

| Model B            |                       |                         |                     |                        |                     |                           |                |
|--------------------|-----------------------|-------------------------|---------------------|------------------------|---------------------|---------------------------|----------------|
| Name               | ${}^1F_{ob(2-10keV)}$ | ${}^1F_{ob(20-100keV)}$ | ${}^2N_H$           | ${}^3\Gamma$           | ${}^4C$             | ${}^5\chi_r^2/\text{dof}$ | ${}^6P_{null}$ |
| QSO B0836+710      | 4.0                   | 4.9                     | $0.07 \pm 0.02$     | $1.353 \pm 0.005$      | $0.28 \pm 0.03$     | 1.02/2421                 | 0.206          |
| 1ES 0033+595       | 1.2                   | 1.5                     | $0.20 \pm 0.02$     | $2.47 \pm 0.05$        | $3.5 \pm 0.8$       | 0.81/229                  | 0.985          |
| PKS 0537-286       | 0.5                   | 2.3                     | $0.30 \pm 0.05$     | $1.22 \pm 0.01$        | $0.7 \pm 0.2$       | 1.03/972                  | 0.235          |
| PKS 2149-307       | 0.6                   | 4.8                     | $< 0.05$            | $1.45 \pm 0.01$        | $2.1 \pm 0.5$       | 0.99/849                  | 0.543          |
| Swift J1656.3-3302 | 0.5                   | 2.0                     | $7.9^{+5.1}_{-3.8}$ | $1.66^{+0.22}_{-0.20}$ | $1.9^{+1.7}_{-0.9}$ | 1.03/42                   | 0.422          |
| IGR J22517+2218    | 0.2                   | 3.5                     | $3.6^{+3.3}_{-2.2}$ | $1.66^{+0.21}_{-0.19}$ | $7.1^{+6.7}_{-3.4}$ | 0.85/49                   | 0.770          |
| Bl Lac             | 0.5                   | 2.3                     | $0.20 \pm 0.07$     | $2.01^{+0.17}_{-0.16}$ | $4.3^{+2.8}_{-1.7}$ | 0.81/31                   | 0.762          |
| 3C 279             | 0.5                   | 2.2                     | $0.04 \pm 0.02$     | $1.75 \pm 0.06$        | $2.5^{+0.7}_{-0.6}$ | 1.07/79                   | 0.311          |

<sup>1</sup> Observed flux in the 2 – 10 keV (or 20 – 100 keV) energy range in units of  $10^{-11}$  erg  $\text{cm}^{-2}$   $\text{s}^{-1}$ . <sup>2</sup> Intrinsic column density of hydrogen in units of  $10^{22}$   $\text{cm}^{-2}$ . <sup>3</sup> Photon index, related to the spectral index  $\alpha$  (where  $F_\nu \propto \nu^{-\alpha}$ ) by  $\alpha = \Gamma - 1$ . <sup>4</sup> IBIS/MOS, BAT/MOS or IBIS/XRT cross-calibration constant. <sup>5</sup> Reduced chi-squared to degrees of freedom. <sup>6</sup> Null hypothesis probability that is the probability of getting a value of  $\chi^2$  as large or larger than observed if the model is correct. If this probability is small then the model is not a good fit to the data.

**Table 6.** Best fit parameters of a broken power-law model in 0.2-100 keV energy range.

| Model C            |                       |                         |  |                        |                     |                           |                |
|--------------------|-----------------------|-------------------------|--|------------------------|---------------------|---------------------------|----------------|
| Name               | ${}^1F_{Ob(2-10keV)}$ | ${}^1F_{Ob(20-100keV)}$ | ${}^7\Gamma_{1,\Gamma_2}$                        | ${}^8E_b$              | ${}^4C$             | ${}^5\chi_r^2/\text{dof}$ | ${}^6P_{null}$ |
| QSO B0836+710      | 4.0                   | 4.9                     | $1.26^{+0.01}_{-0.02}$<br>$1.354 \pm 0.005$      | $0.98 \pm 0.08$        | $0.28 \pm 0.03$     | 1.02/2420                 | 0.274          |
| 1ES 0033+595       | 1.2                   | 1.6                     | $1.38^{+0.16}_{-0.13}$<br>$2.37^{+0.06}_{-0.05}$ | $1.39^{+0.12}_{-0.10}$ | $2.8^{+0.7}_{-0.6}$ | 0.85/228                  | 0.947          |
| PKS 0537-286       | 0.5                   | 2.3                     | $0.83^{+0.09}_{-0.12}$<br>$1.21 \pm 0.01$        | $0.72 \pm 0.09$        | $0.7 \pm 0.2$       | 1.03/971                  | 0.282          |
| PKS 2149-307       | 0.6                   | 4.8                     | $1.47^{+0.01}_{-0.02}$<br>$1.41^{+0.04}_{-0.34}$ | $2.7^{+4.5}_{-1.1}$    | $1.9 \pm 0.5$       | 0.99/848                  | 0.579          |
| Swift J1656.3-3302 | 0.6                   | 2.0                     | $1.03^{+0.17}_{-0.47}$<br>$1.96^{+0.30}_{-0.27}$ | $8.3^{+45.5}_{-3.4}$   | $1.8^{+2.2}_{-1.4}$ | 0.87/41                   | 0.708          |
| IGR J22517+2218    | 0.2                   | 3.5                     | $0.58^{+0.49}_{-0.69}$<br>$1.69^{+0.23}_{-0.19}$ | $1.19^{+0.27}_{-0.26}$ | $7.8^{+8.4}_{-3.7}$ | 0.82/48                   | 0.803          |
| Bl Lac             | 0.5                   | 2.2                     | $1.06^{+0.57}_{-0.73}$<br>$2.02^{+0.34}_{-0.12}$ | $1.71^{+0.75}_{-0.15}$ | $4.6^{+1.7}_{-1.0}$ | 0.89/30                   | 0.633          |
| 3C 279             | 0.5                   | 2.2                     | $1.46^{+0.10}_{-0.11}$<br>$1.78 \pm 0.06$        | $1.16^{+0.27}_{-0.20}$ | $2.7^{+0.8}_{-0.7}$ | 1.01/78                   | 0.446          |

<sup>1</sup> Observed flux in the 2-10 keV (or 20-100 keV) energy range in units of  $10^{-11}\text{ergcm}^{-2}\text{s}^{-1}$ . <sup>4</sup> IBIS/MOS, BAT/MOS or IBIS/XRT cross-calibration constant. <sup>5</sup> Reduced chi-squared to degrees of freedom. <sup>6</sup> Null hypothesis probability that is the probability of getting a value of  $\chi^2$  as large or larger than observed if the model is correct. If this probability is small then the model is not a good fit to the data. <sup>7</sup> Spectral index below the break ( $\Gamma_1$ ) and above the break ( $\Gamma_2$ ). <sup>8</sup> Observed break energy in units of keV.

**Table 7.** Best fit parameters of a broken power-law model with an absorption in excess in 0.2-100 keV energy range.

| Model D      |                       |                         |                     |   |                        |                     |                           |                |
|--------------|-----------------------|-------------------------|---------------------|---|------------------------|---------------------|---------------------------|----------------|
| Name         | ${}^1F_{Ob(2-10keV)}$ | ${}^1F_{Ob(20-100keV)}$ | ${}^2N_H$           | ${}^7\Gamma_{1,\Gamma_2}$                 | ${}^8E_b$              | ${}^4C$             | ${}^5\chi_r^2/\text{dof}$ | ${}^6P_{null}$ |
| PKS 1830-211 | 1.4                   | 4.3                     | $1.5^{+0.2}_{-0.1}$ | $0.95 \pm 0.05$<br>$1.32^{+0.10}_{-0.07}$ | $4.01^{+0.42}_{-0.54}$ | $0.8^{+0.3}_{-0.2}$ | 1.06/856                  | 0.101          |

<sup>1</sup> Observed flux in the 2 – 10 keV (or 20 – 100 keV) energy range in units of  $10^{-11}\text{erg cm}^{-2}\text{s}^{-1}$ . <sup>2</sup> Intrinsic column density of hydrogen in units of  $10^{22}\text{cm}^{-2}$ . <sup>4</sup> IBIS/MOS, BAT/MOS or IBIS/XRT cross-calibration constant. <sup>5</sup> Reduced chi-squared to degrees of freedom. <sup>6</sup> Null hypothesis probability that is the probability of getting a value of  $\chi^2$  as large or larger than observed if the model is correct. If this probability is small then the model is not a good fit to the data. <sup>7</sup> Spectral index below the break ( $\Gamma_1$ ) and above the break ( $\Gamma_2$ ). <sup>8</sup> Observed break energy in units of keV.

**Table 8.** Upper limits to  $R$  under the assumption of a pexrav model.

| Name | QSO B0836+710 | 1ES 0033+595 | PKS 0537-286 | PKS 2149-307 | PKS 1830-211 | Swift J1656.3-3302 | IGR J22517+2218 | Bl Lac | 3C 279 |
|------|---------------|--------------|--------------|--------------|--------------|--------------------|-----------------|--------|--------|
| $R$  | 0             | 0            | 0.09         | 0.08         | 0            | 0.5                | 3E-6            | 0      | 3E-4   |

likely the absorbing material is linked to the presence of this component. This working scenario is supported by a theory presented, e.g., in Ferrari (1998), in which the confinement of the radio jet needs the presence of a cold medium (local to the AGN) so that jet expansion is suppressed.

In our sample we have found neither an evidence of an iron emission line at 6.4 keV nor evidence of a Compton reflection "hump" above 10 keV. The lack of these spectral features – interpreted as the result of reprocessing of the primary continuum by cold matter around the X-ray source, presumably the accretion disk (Lightman & White 1988; Guilbert & Rees 1988; George & Fabian 1991; Sambruna & Eracleous 1999; Sambruna, Eracleous & Mushotzky 1999) – can be explained either with the out-and-out absence of reprocessing features in blazar-type objects or with the hypothesis that these features are difficult to be detected in strong radio sources being likely diluted by the jet (Sambruna et al. 2006).

There is also evidence that the spectral shape does not change between 0.2–10 keV and 20–100 keV energy ranges, supporting the idea that, above 10 keV, no additional component to the power-law (e.g. Compton reflection hump) is present in the spectrum.

The value of the cross-calibration constant (see Tables B and C) shows that a strong flux variability is present in QSO B0836+710, 1ES 0033+595, PKS 1830-211, IGR J22517+2218, BL Lac, and 3C 279. In particular, we derived that IGR J22517+2218 showed severe intensity changes between the INTEGRAL and the Swift observations with a value of the XRT/IBIS inter-calibration factor of about 7. This is not a surprise because of the nature of the object and data being not simultaneous. In addition, we remark that INTEGRAL/IBIS data set correspond to an average performed on observations spanning on 3 years, while the data for the low-energy range (XMM and XRT) correspond to observations with a time baseline of few hours.

### 3.3 PARAMETER DISTRIBUTIONS AND CORRELATIONS

Although the number of sources of our sample is not large, we have also analyzed the distribution of the spectral parameters (absorbing column density, spectral index, redshift) and their possible correlations. This type of analysis has been performed, so far, only between 0.2 – 10 keV (Yuan et al. 2006). Our study is still preliminary and has been performed with a detailed comparison among the results of our own spectral analysis and those already available in literature in a limited energy range. The reference sample includes 35 RL objects – with 19/35 sources identified as blazars – (Galbiati et al. 2005; Page et al. 2005; Yuan et al. 2006) and shows an absorption of unknown intrinsic nature. In order to avoid any problem of "orientation dependence bias" when studying the  $N_H$  and  $\Gamma$  distribution, we have selected, from the quoted sample, only the blazar-type objects. In particular, for the  $N_H$  study we have accounted for the blazars with a specific value of the intrinsic absorption (we have not accounted for the upper limits on  $N_H$ ), obtaining a sub-sample of 16 objects.

In the framework of a possible  $N_H$ -redshift relation, we also combined our results with the larger sample of RL objects (Galbiati et al. 2005; Page et al. 2005; Yuan et al.

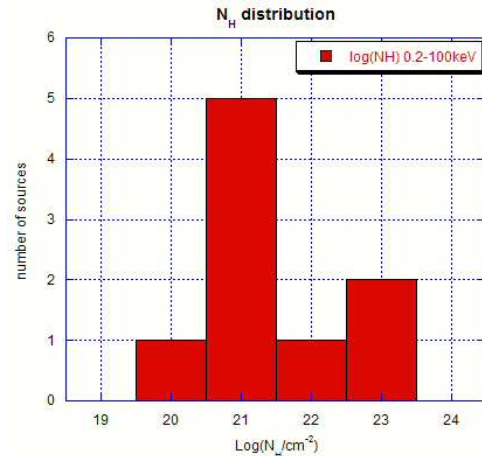


**Figure 2.** Distribution of the X-ray absorption column density ( $N_H$ ) for our sample objects over the 0.2 – 100 keV energy range.

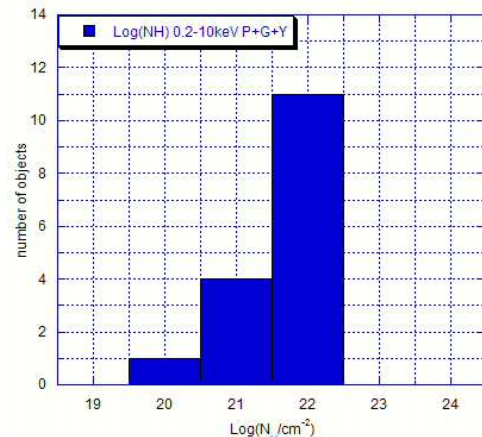


**Figure 3.** The  $N_H$  distribution of a larger sample of 16 blazars over the 0.2 – 10 keV energy range. See text for more details.

2006), counting out three sources belonging to our sample (QSO B0836+710, PKS 2149-307 and PKS 0537-286). In fact, it is interesting to check whether the 9 selected blazars in the sample and analyzed in a more wide energy band, follow the trend of  $N_H$  with the redshift previously found by Yuan et al. (2006). If this would be the case, we would have further evidence that the absorbing column density, in these sources, is linked to the distance and thus a confirmation of a cosmic evolution effect.

#### 3.3.1 ABSORPTION DISTRIBUTION

We made a detailed analysis of the rest-frame hydrogen column density for our selected blazars, in conjunction with the intervening absorption in excess to the galactic one.

The  $N_H$  distribution shown in Figure 2 appears to be asymmetric, with a peak located at about  $\text{log}(N_H) = 21$  and tails extending towards low and high values up to  $\text{log}(N_H) = 20$  and  $\text{log}(N_H) = 23$ , respectively. It is worth to note that the statistical significance of this result is strongly affected by the limited number of objects in our sample. Therefore we compare our sample with the larger sub-sample

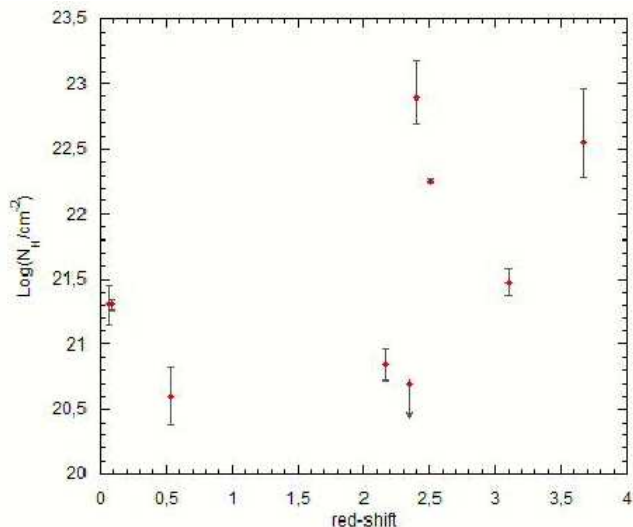


**Figure 4.** The X-ray absorption column density  $N_H$  as a function of the redshift for our sample.

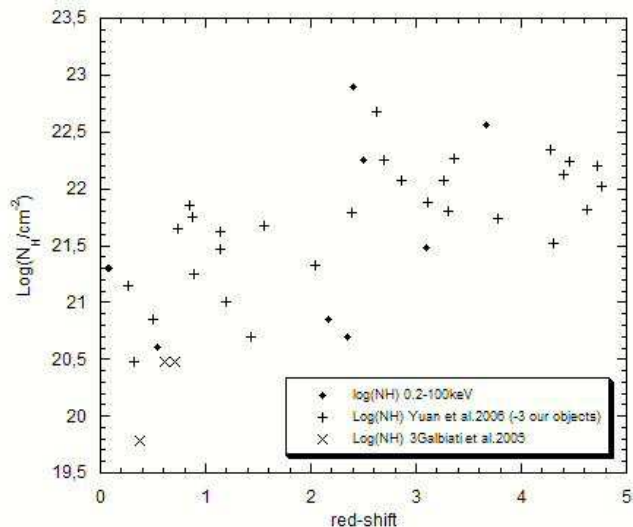


**Figure 5.** The X-ray absorption column density  $N_H$  as a function of the redshift, combining the results of our sources (filled rhombs) and the ones of a larger sample (plus and cross signs) analyzed in the soft X-ray energy range.

from the literature observed in the 0.2–10 keV energy range from XMM-Newton that includes 16 RL objects identified as blazars and with a specific value of the absorption. We underline that this one includes only one object belonging to our sample (the blazar QSO B0836+710). The  $N_H$  distribution of the larger sample is shown in Figure 3, with a peak located at  $\log(N_H) = 22$  and a tail extending towards lower values up to  $\log(N_H) = 20$ . Comparing the distributions in Figure 3 and in Figure 2, we note that sources with absorbing column density around  $\log(N_H) = 23$  are “missing”. This evidence is expected in view of the fact that in the soft X-ray energy range (0.2–10 keV) the sources with an absorbing column density  $N_H \geq 1.3 \cdot 10^{23} \text{ cm}^{-2}$  are almost completely obscured.

This occurrence strongly suggests that data above 10

keV represent a crucial tool to construct an unbiased selection of heavily absorbed objects.

The  $N_H$ -redshift trend of our sample is shown in Figure 4.

The comparison of this  $N_H$ - $z$  plot with those previously analyzed by Yuan et al. (2006) at various redshifts for a sample of 32 RL sources, seems to indicate that the property of the X-ray absorbing gas evolves with cosmic time. This trend is shown in Figure 5, where we added 3 objects analyzed by Galbiati et al. (2005). In fact, at first glance, a correlation between  $N_H$  and redshift seems to exist and, compared to low redshifts ( $z < 2$ ), a shift toward higher values of  $N_H$  seems to be indicated at high redshifts.

The sample of 32 sources includes 3 objects of our sample (QSO B0836+710, PKS 0537-286 and PKS 2149-307) and the  $N_H$  values for these 3 sources as obtained through our spectral analysis are in agreement with those presented in the work of Yuan and collaborators (2006).

The existence of a correlation is also confirmed by the statistical analysis: we obtain a correlation coefficient ( $R$ ) around 0.7 (Figure 5), when the results corresponding to our sample are added to the sources investigated by Page et al. (2005), Galbiati et al. (2005) and Yuan et al. (2006).

All together these results seem to support the hypothesis of an intrinsic absorber. Three further hints support its intrinsic nature:

- the existence of a spatial isotropy of the inter-galactic absorbers is most unlikely;
- the X-ray absorption is associated with RL but not with RQ objects (Yuan & Brinkmann 1999). This evidence supports the hypothesis that the absorber are physically associated with the RL quasars;
- the change of the  $N_H$  distribution that seems to occur at  $z \sim 2$  and the decrease of the slope in the  $N_H$ - $z$  relation at  $z > 2$  could indicate an effect of cosmic evolution. This effect could be due, e.g., to a rate of stellar formation. In fact, an increase of the stellar formation at  $z \leq 2$  could reduce the amount of gas in the host galaxy.

### 3.3.2 PHOTON-INDEX DISTRIBUTION

The photon-index distribution was then investigated by adding the FSRQ 3C 273 and 4C 04.42 in our analysis ( $\Gamma \sim 1.6$  and  $\sim 1.3$ , respectively, as obtained by our broadband analysis). The  $\Gamma$  distribution for the complete sample is shown in Figure 6 and the mean value obtained in 0.2–100 keV energy band is  $\Gamma = 1.39 \pm 0.01$ .

For comparison, in Figure 7 we also show the photon index distribution derived from Page et al. (2005), Galbiati et al. (2005) and Yuan et al. (2006) for 35 sources. The  $\Gamma$  distribution of our sample shows a peak at  $\Gamma \sim 1.4$ , whereas the  $\Gamma$  distribution of the RL objects shows a peak corresponding to a steeper value of  $\Gamma \sim 2$ . However, we note here that our sample is mainly composed by FSRQ, while the larger sample contains different types of RL objects - not all identified as blazars. Therefore, in order to perform a meaningful comparison, we have studied the photon index distribution for sources - in the larger sample - identified as blazars (19 objects). The peak of the  $\Gamma$  distribution (see Figure 8) is, again, around 2.

To account for the fact that most of the sources in our

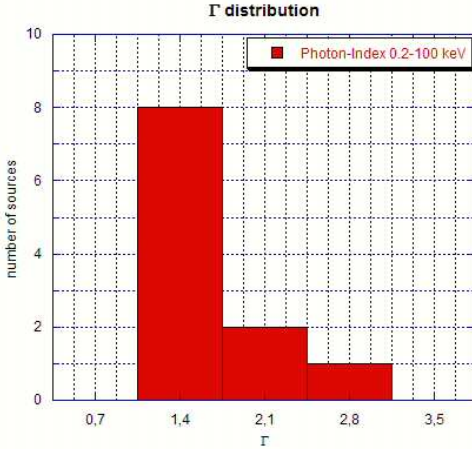


**Figure 6.** Distribution of the power-law photon-index for our sample in the 0.2 – 100 keV energy range.

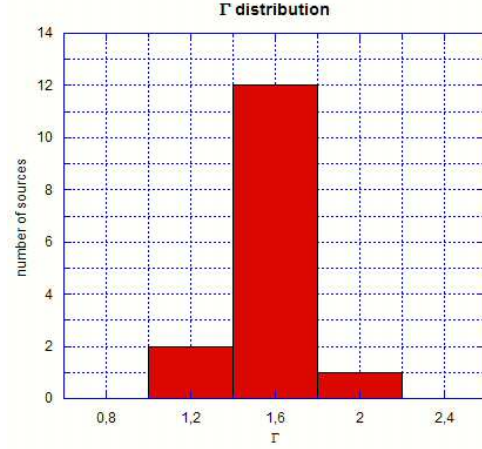


**Figure 9.** Photon-index distribution for 15 sources identified as FSRQ.

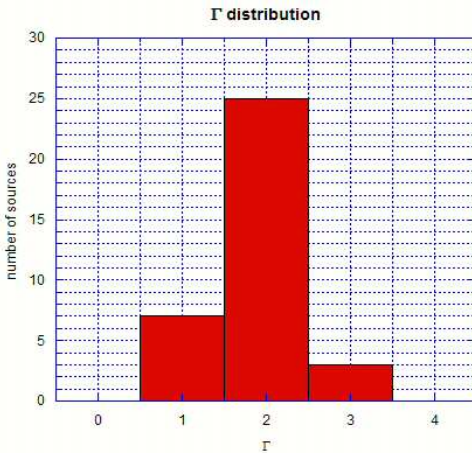


**Figure 7.** Distribution of the photon-index resulting by the analysis performed in the works of Page et al. (2005), Galbiati et al. (2005) and Yuan et al. (2006) and including 35 RL objects.

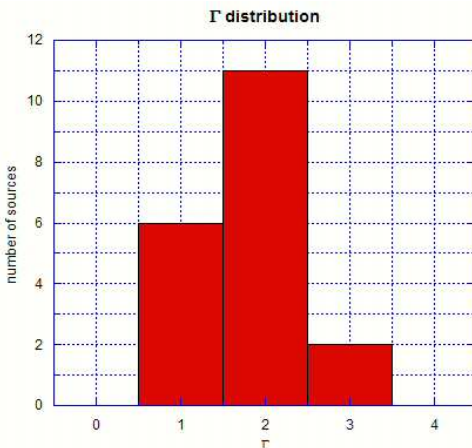


**Figure 8.** Photon-index distribution for 19 sources identified as blazars.

sample are FSRQ-type objects and that FSRQs in X-rays show a lower value of  $\Gamma$  with respect to BL Lac objects, we studied the  $\Gamma$  distribution including only the FSRQ sources (15 objects) in the larger sample. In this case, the  $\Gamma$  distribution in Figure 9 shows a peak at  $\Gamma \sim 1.6$ , a value steeper than that for our blazars sample.

The differences between the values of  $\Gamma$  of our sample and those of the larger sample could be due to the hard X-ray selection of our INTEGRAL/IBIS sample, which is clearly biased towards the flatter values of the photon index.

#### 4 SUMMARY AND CONCLUSIONS

In this work we presented a broad-band X-ray spectral study of a sample of 9 blazars (with a redshift range of  $0.1 < z < 3.7$ ) observed with INTEGRAL, XMM-Newton and Swift. The main results can be summarized as follows:

- The broad-band spectra of all selected sources are well reproduced with a power-law model absorbed by an amount of gas in excess to the Galactic one ( $N_H \sim 10^{20}-10^{23} \text{cm}^{-2}$  in rest-frame of the source; only an upper limit of  $N_H \sim 5 \cdot 10^{20} \text{cm}^{-2}$  has been derived for the FSRQ PKS 2149-307).
- The absorption seems to be a signature of a cold intrinsic absorber, confirming and extending to larger sample previous results quoted in the literature (Cappi et al. 1997; Page et al. 2005; Yuan et al. 2006).
- The present work provides a further confirmation of the existence of a  $N_H$ -redshift trend, obtained for a large sample of RL objects (not only blazars).
- The broad-band analysis of our sample of blazars revealed a harder spectrum with a photon-index of the order of  $\Gamma \sim 1.4$ , compared to the value obtained with the distribution including the FSRQ sources of the larger sample (15 objects). Such a difference could be due to the hard X-ray selection of our INTEGRAL/IBIS sample which is clearly biased towards flatter values of the photon index.
- We have found no evidence of reflection components (reflection “hump” and iron emission line), with the exception of the source IGR J22517+2218 that shows the presence of a weak iron line. This result is expected in blazar-type objects.

In conclusion, the analysis presented here has shown that our INTEGRAL-sample selection favours objects heavily absorbed and with a flatter value of spectral index. On the other hand, the present broad-band analysis of INTEGRAL/IBIS, XMM-Newton and Swift observations of RL QSOs confirms that the observed flattening is common in these objects, and is clearly detected in eight quasars of our sample (8/9). The assumption of an intrinsic origin and a cold nature for the absorber is consistent with previous results up to 10 keV obtained by Page et al. (2005) and Yuan et al. (2006) with XMM-Newton data only. However, a broken power-law model, as an alternative explanation for the deficit of soft photons observed in the majority of our sources, cannot be ruled out by the data.

## ACKNOWLEDGMENTS

Authors acknowledge support from INAF and ASI via contract I/008/07.

## REFERENCES

- Abdo A.A., Ackermann M., Ajello M. et al., 2009, *ApJ*, 700, 597
- Antonucci R., 1993, *ARA&A*, 31, 473
- Arnaud K., 1996, in *ASP Conf. Ser. 101, Astronomical Data Analysis Software and Systems V*, ed. G. Jacoby & J. Barnes (San Francisco: ASP), 17
- Ballantyne D.R., Ross R.R. & Fabian A.C., 2002, *MNRAS*, 332, L45
- Bassani L., Landi R., Malizia A. et al., 2007, *ApJ*, 669, L1
- Bechtold J., Elvis M., Fiore F. et al., 1994, *AJ*, 108, 759
- Bird A.J., Malizia A., Bazzano A. et al., 2007, *ApJ*, 170, 175
- Canizares C.R. & White J.L., 1989, *ApJ*, 339, 27
- Cappi M., Matsuoka M., Comastri A. et al., 1997, *ApJ*, 478, 492
- Chernyakova M., Neronov A., Courvoisier T.J.-L. et al., 2007, *A&A*, 465, 147
- De Rosa A., Piro L., Tramacere A. et al., 2005, *A&A*, 438, 121
- De Rosa A., Bassani L., Ubertini P. et al., 2008, *MNRAS*, 388, 54
- Dermer C.D. & Schlickeiser R., 1993, *ApJ*, 416, 458
- Elvis M., Fiore F., Mathur S. & Wilkes B., 1994, *ApJ*, 425, 103
- Eracleous M., Sambruna R. & Mushotzky R.F., 2000, *ApJ*, 537, 654
- Fabian A.C., Celotti A., Iwasawa K. & Ghisellini G., 2001, *MNRAS*, 324, 628
- Fall S.M. & Pei Y.C., 1995, *Proceedings of the ESO Workshop Held at Garching, Germany, 21-24 November 1994*, edited by G. Meylan. Springer-Verlag Berlin Heidelberg New York. Also *ESO Astrophysics Symposia*, p.23
- Ferrari A., 1998, *A&A*, 36, 539
- Fiore F., Giommi P., La Franca F. et al., 1998, *arXiv:astro-ph/9911149*
- Galbiati E., Caccianiga A., Maccacaro T. et al., 2005, *A&A*, 430, 927
- George I.M. & Fabian A.C., 1991, *MNRAS*, 249, 352
- Giuliani A., D'Ammando F., Vercellone S. et al., 2009, *A&A*, 494, 509
- Goldwurm A. et al., 2003, *A&A*, 411, 223
- Grandi P., Maraschi L., Urry C.M. & Matt G., 2001, *ApJ*, 556, 35
- Grandi P. & Palumbo G.C., 2004, *Science*, 306, 998
- Grandi P., Malaguti G. & Fionchi M., 2006, *ApJ*, 642, 113
- Grupe D., Mathur S., Wilkes B. & Osmer P., 2006, *AJ*, 131, 55
- Guilbert P.W. & Rees M.J., 1988, *MNRAS*, 233, 475
- Kirsch M.G.F., Becker W., Larsson S. et al., 2004, *ESASP*, 552, 863
- Kirsch M.G.F., Briel U.G., Burrows D. et al., 2005, *SPIE*, 5898, 22
- Lawson A.J. & Turner M.J.L., 1997, *MNRAS*, 288, 920
- Lebrun F., Leray J.P., Lavocat P. et al., 2003, *A&A*, 411, 141
- Lightman A.P. & White T.R. 1988, *ApJ*, 335, 57
- Magdziarz P. & Zdziarski A.A. 1995, *MNRAS*, 273, 837
- Maraschi L., Ghisellini G. and Celotti A., 1992, *ApJ*, 397, L5
- Masetti N., Palazzi E., Bassani L. et al., 2004, *A&A*, 426, 41
- Masetti N., Mason E., Morelli L. et al., 2008, *A&A*, 482, 113
- Matt G., 2001, *AIPC*, 599, 209
- O'Flaherty K.S. & Jakobsen P., 1997, *ApJ*, 479, 673
- Padovani P., 1997, *MmSAI*, 68, 47
- Page K.L., Turner M.J.L., Reeves J.N. et al., 2003, *MNRAS*, 338, 1004
- Page K.L., Reeves J.N., O'Brien P.T. & Turner M.J.L., 2005, *MNRAS*, 364, 195
- Pittori C., Verrecchia F., Chen A.W. et al., 2009, *A&A* 506, 1563
- Reimers D., Bade N., Schartel N. et al., 1995, *A&A*, 296, 49
- Sambruna R.M. & Eracleous M., 1999, *arXiv:astro-ph/9911503*
- Sambruna R.M., Eracleous M. & Mushotzky R.F., 1999, *ApJ*, 526, 60
- Sambruna R.M., Gliozzi M., Tavecchio F. et al., 2006, *ApJ*, 652, 146
- Siebert J., Brinkmann W., Morganti R. et al., 1996, *MNRAS*, 279, 1331
- Sikora M., Begelman M.C. & Rees M.J., 1994, *ApJ*, 421, 153
- Stickel M., Padovani P., Urry C.M., Fried J.W., & Kuhr H., 1991, *ApJ*, 374, 431
- Tavani M. et al. 2008, *Nucl. Instrum. Methods Phys. Res. A*, 588, 52
- Tavecchio F., Maraschi L., Ghisellini G. et al., 2007, *ApJ*, 665, 980
- Ubertini P., Lebrun F., Di Cocco G. et al., 2003, *A&A*, 411, 131
- Urry M.C. & Padovani P., 1995, *PASP*, 107, 803
- Vignali C., Brandt W.N., Schneider D.P. et al., 2003, *AJ*, 125, 2876
- Vignali C., Brandt W.N., Schneider D.P. and Kaspi S., 2005, *AJ*, 129, 2519
- Zhang S., Chen Y., Collmar W. et al., 2008, *ApJ*, 683, 400
- Zwaan M.A., Verheijen M.A.W. & Briggs F.H., 1999, *PASA*, 16, 100

- Yuan W., Brinkmann W., Siebert J. & Voges W., 1998, A&A, 330, 108
- Yuan W. & Brinkmann W., 1999, Proceedings of the Symposium "Highlights in X-ray Astronomy", eds. B. Aschenbach & M.J. Freyberg, MPE Report 272, 240
- Yuan W., Fabian A.C., Worsley M.A. & McMahon R.G., 2006, MNRAS, 368, 985